Earth as an exoplanet mission concept for a lunar orbiting cubesat

Ana I. Gómez de Castro,[a,*] Leire Beitia-Antero,[a] Carlos E. Miravet-Fuster,[b] Lorenzo Tarabini,[b] Albert Tomás,[b] Juan C. Vallejo,[a] Ada Canet,[a] Mikhail Sachkov,[c] and Shingo Kameda[d]
[a]Universidad Complutense de Madrid, Faculty of Mathematics, AEGORA Research Group, Madrid, Spain
[b]SENER, Ingeniera y Sistemas, Barcelona, Spain
[c]Institute of Astronomy of the Russian Academy of Sciences, Moscow, Russia
[d]Rikkyo University, Department of Physics, Tokyo, Japan

Abstract. There is a growing interest in lunar exploration fed by the perception that the Moon can be made accessible to low-cost missions in the next decade. The ongoing projects to set a communications relay in lunar orbit and a deep space gateway, as well as the spreading of commercial-of-the shelf technology for small space platforms such as the cubesats contribute to this perception. Small, cubesat size satellites orbiting the Moon offer ample opportunities to study the Moon and enjoy an advantage point to monitor the Solar System and the large-scale interaction between the Earth and the solar wind. We describe the technical characteristics of a 12U cubesat to be set in polar lunar orbit for this purpose and the science behind it. The mission is named Earth as an exoplanet (EarthASAP) and is submitted to the Lunar Cubesats for Exploration call in 2016. EarthASAP is designed to monitor hydrated rock reservoirs in the lunar poles and to study the interaction between the large Earth's exosphere and the solar wind in preparation for future exoplanetary missions. [DOI: 10.1117/1.JATIS.5.4.044004]

Keywords: space vehicles; space vehicles: instruments; Moon; Earth; meteorites, meteors, meteoroids; comets: general.

Paper 19062 received May 31, 2019; accepted for publication Oct. 1, 2019; published online Oct. 23, 2019.

1 Introduction

Cubesat technology started back in 1999. At that time, California Polytechnic State University and Stanford University produced the basic cubesat specifications as an attempt to facilitate the design, manufacture, and testing of small satellites.[1] Cubesats are modular structures with unit (1U) of dimensions $10 \times 10 \times 10$ cm^3 and weight smaller than 1.5 kg that use commercial-of-the-shelf (COTS) products. Usually, they are stacked in 2U, 3U up to 20U platforms originally intended for low Earth orbit where the electronic components are not submitted to the hard environment of interplanetary space.

The increasing interest on lunar exploration and the on-going initiative to build the Deep Space Gateway[2] has open the path to the development of lunar cubesats (LUCE). This new generation will need to confront important challenges such as the adaptation to interplanetary space or the development of communication strategies based on shared communications relays. Moon's orbit offers ample opportunities to study the Moon and enjoys an advantage point to monitor the Solar System and the large-scale interaction between the Earth and the solar wind.

In recognition of this interest, the European Space Agency (ESA) focused the 2016 SysNova call on LUCE; ESA's SysNova calls open regularly[3] aiming at getting innovative proposals in space technology. LUCE Sysnova technical challenge was intended to address four different topics: lunar resource prospecting, environment and effects, science from or in the Moon, and lunar exploration technology and operations demonstration. The first version of the project we present in this paper was submitted to this call, and although it was not selected, it evolved and matured to address some critical challenges such as the required instrument miniaturization, the propulsion for orbit maintenance, or the on-board autonomy assuming sparse communication windows to an international communication relay. The project was named Earth as an exo-planet (EarthASAP) as one of its key scientific objectives is using the lunar orbit vantage point to monitor the interaction between the Earth's exosphere and magnetosphere with the solar wind, also in preparation for the coming exoplanetary research missions.

In the following sections, the scientific objectives (Sec. 2), the mission concept (Sec. 3), the mission and data handling (Sec. 4) are described. This paper concludes with a brief summary together with the risk evaluation and the palliative solutions proposed by the team (Sec. 5).

2 Scientific Objectives

EarthASAP is intended to be in lunar polar orbit and run three research programs: the observation of the Earth's magnetosphere and exosphere, the detection of diffuse matter within the heliosphere (comets, asteroids, and dusty clouds) and the monitoring of the water content and space weather in the lunar poles.

2.1 *Earth Interaction with the Solar Wind*

There is increasing evidence of the coupling between the upper atmospheric layers (upper thermosphere) to the plasmasphere, to the magnetosphere, and to space weather conditions.[4] At the base of the exosphere, a population of energetic hydrogen atoms is generated as a result of this coupling. This layer is critical to understand the Earth's thermal flow and particle escape, i.e., the planetary wind, as well as its relationship with solar activity.

*Address all correspondence to Ana I. Gómez de Castro, E-mail: aig@ucm.es

2329-4124/2019/$28.00

The most sensitive tracer to measure the distribution of exospheric hydrogen is the Lyman α (Lyα) transition. Space probes such as the imager for magnetopause-to-aurora global exploration (IMAGE)[5] or the two wide-angle imaging neutral-atom spectrometers (TWINS)[6] mission have used Lyα to derive the distribution of hydrogen while navigating within the exosphere. The GEO instrument[7] on board IMAGE found that the particle density does not decrease exponentially with the distance to the Earth as predicted by the classical models.[8] In fact, the density distribution is bimodal with a dominant component peaking at 1 R_E and an extended component reaching $n_H = 20$ cm^{-3} at 8 R_E.[9] This result was further confirmed by the ultraviolet imaging spectrograph[10] experiment on board the Cassini spacecraft. During Cassini's Earth swing by, the solar Lyα radiation scattered by the neutral hydrogen atoms of the geocorona was shown to trace an extended exosphere around the Earth.[11] Later on, TWINS obtained the 3-D distribution of Lyα emission within 8 R_E (and above 3 R_E) around the Earth and measured even higher density values[12] (see Fig. 1). The recent images obtained by the Japanese Space Agency with the proximate object close flyby with optical navigation (PROCYON) probe show that the Earth's exosphere extends further than 38 R_E.[14] Extended exospheres have also been detected in Venus and Mars[15] and this seems to be a common characteristic of terrestrial planets.

Both IMAGE/GEO and TWINS reported variations in the hydrogen distribution by about $\pm 20\%$ with time that apparently is not controlled by any solar quantity or geomagnetic parameter alone.[16] A systematic monitoring of the Earth's hydrogen envelope and escape is necessary to determine the processes controlling this evolution. The exosphere is mainly composed by neutral hydrogen that interacts very weakly with the diffuse solar wind and the Earth's magnetic field. The exospheric ionization fraction is mainly controlled by the charge-exchange reactions between the neutral exospheric atoms and the fast charged particles accelerated by the geomagnetic field. The higher the ionization fraction, the more efficient is the solar wind in the removal of exospheric gas. A systematic long-term monitoring of the Earth's hydrogen envelope and escape from outside of geocorona is necessary to determine the processes acting on the response of the exosphere to geostorms.

Missions like IMAGE or TWINS have been orbiting the Earth within the magnetospheric cavity (the cavity size is about 70,000 km toward the Sun and extends as far as 1000 R_E toward the anti Sun, where the magnetotail is located). As a result, the interpretation of the data has been hampered by the difficulties to determine the Lyα emission within a complex geometry and to measure at the same time the solar flux and the heliospheric background. This issue is critical since the exospheric emission at large R_E drops below the background Lyα radiation. As an example, at 10 R_E, the ratio of exospheric to background Lyα radiation ranges between 0.21 and 1.17 depending on the strength of the variable background (estimate based on data from IMAGE[9]). The images obtained by the Lyman alpha imaging camera (LAICA) on-board the PROCYON satellite show the potentials of wide-field imaging from large distances to capture the faint exospheric emission above the heliospheric background.

EarthASAP is designed to map the exosphere from outside, measuring simultaneously the exospheric emission and the variable background obtaining very accurate measurements of the hydrogen distribution at large Earth radii. This is feasible at a low cost using the Moon as a stable gravitational platform to orbit the Earth. A 3-D image of the Earth's exosphere and magnetosphere can be constructed in one synodic month.

EarthASAP's key objective is measuring the Lyα source function at scales as small as 0.1 R_E (3 arc min) and to resolve the contributions to the line excitation from solar radiation and other processes, such as collisions with high-energy particles from the Sun or from internal magnetospheric sources, including the radiation belts. Moreover, EarthASAP is designed to map the exosphere/magnetosphere radiation produced by neutral oxygen (OI) and ionized helium (HeII, $n = 2$ to 3 resonance transition at 164 nm). Oxygen is expected to be abundant in Earth-like planets but even for the Earth, its exospheric distribution is poorly known at large Earth radii; oxygen is also the most highly referenced astronomical biosignature gas. All the target tracers for the EarthASAP mission, HI, OI, and HeII, are also important tracers of energetic neutral atoms (ENAs). ENAs are created in charge-exchange collisions between hot plasma ions (protons and alpha particles) and the cold neutral gas in the magnetospheric/exospheric environment. Therefore, the spatial distribution of ENAs emission indicates the location of frequent collisions with fast particles (solar wind, magnetic reconnection regions, and radiation belts) and can be used as a tracer of these phenomena. The wide-field imaging and the rapid read out of EarthASAP is designed to enable monitoring

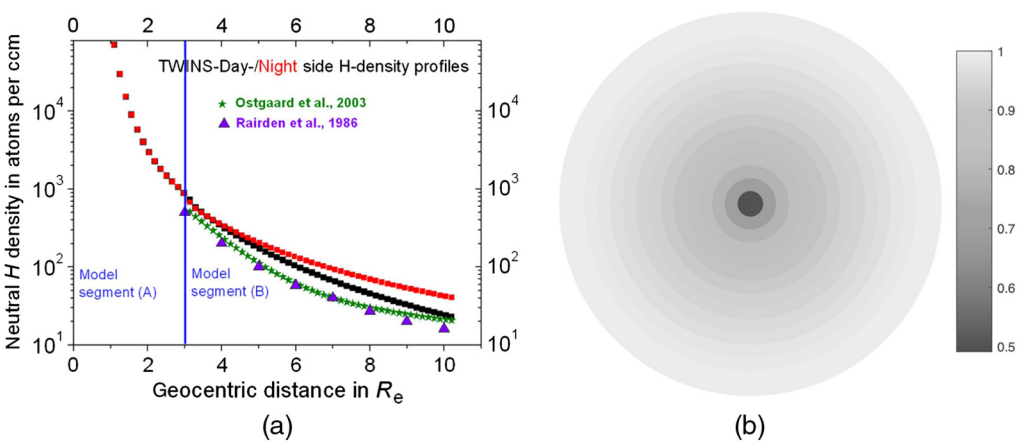

Fig. 1 (a) Radial distribution of hydrogen in the Earth's exosphere as derived from the Lyα measurements obtained by the TWINS mission[12] and (b) transmissivity of the Earth (including exosphere) to background Lyα radiation; the radius is 15 R_E.[13]

variable phenomena and isolate their contribution to the total radiative budget.

2.1.1 *Connection with exoplanetary research*

The detection of exoplanets has opened the possibility of studying planetary exospheres and atmospheric escape in planetary systems submitted to very different stellar radiation fields and space weather conditions. The transit of planetary exospheres in front of the stellar disk produces a net absorption that has been detected in the stellar Lyα profile of large, massive planets in close orbit around their parent stars: HD 209458b,[17] HD 189733b,[18] and GJ 436b.[19,20] The next step is measuring atmospheric escape in Earth-like exoplanets. The first evaluations are promising, especially for planets orbiting in the habitable zone around M-type stars.[13] The high optical depth of the Lyα line results in very low-gas columns ($N_H > 5 \times 10^{17}$ cm^{-2}) being sufficient to block the Lyα radiation from the star without producing noticeable effects in the rest of the stellar spectral tracers.[21] The radius, at which Lyα becomes optically thick $\tau_{Ly} > 1$, sets the geometric cross section of the planet to the Lyα radiation which is significantly larger than the planet itself. As a result, the transit duration and the shape of the Lyα light curve depend strongly on exospheric properties. Observations of exoplanetary Lyα transits will enable understanding the interaction of the Earth's atmosphere with the Sun at the time when life emerged on Earth, an uncertain date between 2.7 and 4.3 Gyr ago.[22] In preparation for these activities, a better understanding of the Earth's environment is required.

2.1.2 *Earth observations during lunar total eclipses*

During the next lunar eclipses of November 8, 2022 and June 26, 2029, there will be a unique chance to observe the Earth's exosphere while transiting the solar disk (see Fig. 2). This viewing angle will provide exclusive information on the scattering and absorption of solar photons by the uppermost layers of the Earth's atmosphere to compare with the theoretical predictions of the Lyα light curves.

2.2 *Diffuse Matter Within the Heliosphere: Comets, Asteroids, and Dusty Clouds*

The resonant scattering of solar Lyα photons by neutral hydrogen within the heliosphere produces a bright far ultraviolet background first reported from OGO-5 data.[23,24] The slow flow of hydrogen atoms comes from the local interstellar cloud (LIC); as the Solar System crosses the LIC, the heliosphere creates a shock front that only neutral particles can penetrate. The shock front is at 94 AU from the Sun[25] in the upwind direction, ecliptic longitude (J2000) 225.4 deg $\pm$ 0.5 deg and latitude 5.1 deg $\pm$ 0.2 deg.[26] The heliospheric Lyα intensity varies as the Sun rotates, especially at low latitudes since the Sun's ultraviolet emission is enhanced in localized active regions; however, variations occur at a slow pace.[27]

Surveying systematically the heliosphere in Lyα enables the detection and study of comets photoevaporation. Lyα observations are an ideal tool for searching for comets since neutral hydrogen is the main component of the coma. These observations can be used to derive the water production rate of the comet as a function of time.[28,29] EarthASAP is designed to grow on the experience of SOHO/SWAN providing higher angular resolution (0.05 deg instead of 1 deg) and a wide field of view to study the detailed structure of the evaporation process and the interaction of the coma with the heliospheric magnetic field. This extra angular resolution will result in an enhanced detectability since cometary tails are clumpy structures. High-resolution imaging of hydrogen distribution in the comet envelop and tail is a very sensitive probe to study comets' photoevaporation and ionization by solar photons. Moreover, the tail interacts with the solar wind through magnetic processes and charge-exchange reactions; hence, UV observations are very useful to study the solar wind properties along the path of the comet.[30] EarthASAP angular resolution is designed to be similar to that of ALICE.[31]

The far ultraviolet range is very sensitive to small dust columns. As a result, dust clouds in the Earth–Moon environment can be monitored such as those located in the libration points or those associated with small bodies streams such as the Orionids, Taurids, or Leonids orbits.

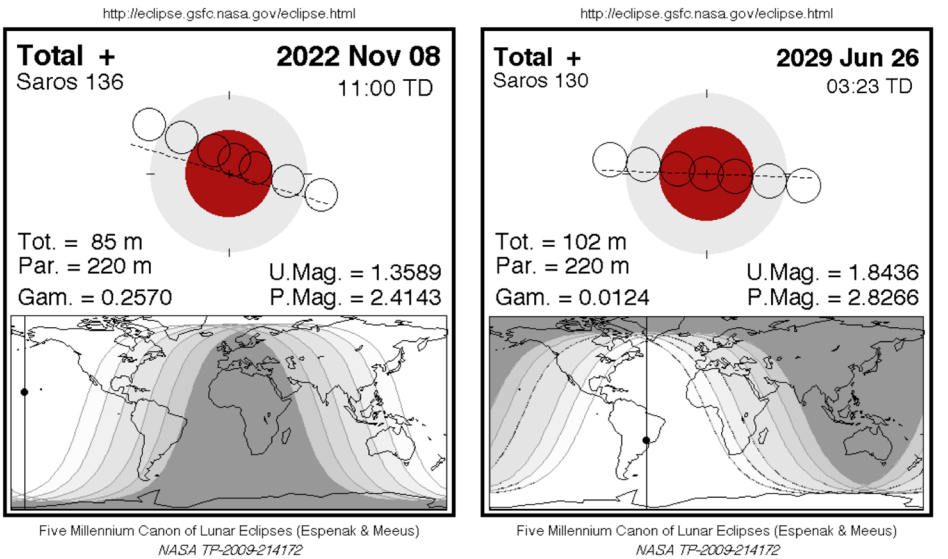

Fig. 2 Earth–Moon configuration during the next total lunar eclipses: November 8, 2022, and June 26, 2029. At central eclipse, the Earth, the Moon, and the Sun are nearly aligned enabling a unique observation of the Earth's geocorona from lunar orbit.

2.3 *Water Content and Space Weather in the Moon Poles*

Future lunar settlements will be most likely be sited on the Moon poles. Thus it is crucial to determine the abundance of the water content in hydrated rocks. The instrument Lyman alpha mapping project (LAMP) on board the lunar reconnaissance orbiter[32] mapped the hydration and weathering of the lunar terrain by measuring the slope of the UV spectrum in 164- to 190-nm range.[33] The presence of a strong water absorption edge in the far-UV (near 165 nm) enables the study of lunar hydration by a simple linear fitting of the reflectance spectrum in the 164- to 173-nm range, where even the small water abundance affects significantly the slope. As shown in Fig. 3, significant variations are detected with latitude; these variations are compared with the slope in the 175- to 190-nm range that it is not affected by hydration effects. In fact, the analysis of LAMP dayside data shows that the 175- to 190-nm region is a good indicator of weathering and composition.[34] The steeper (redder) slopes are consistent with increased hydration earlier and later in the day, and at higher latitudes.

EarthASAP is designed to monitor the poles with a wide field of view (roughly 174 km × 262 km) per image and a resolution of ∼430 m. Though LRO/LAMP images have better resolution (down to 100 m),[35] EarthASAP's wide field of view makes feasible differential measurements of the far UV emission variability and hence, of the variations of surface ice and frost in the polar regions. In Fig. 4, the procedure is illustrated from the images obtained by LRO/LAMP of the south lunar pole.

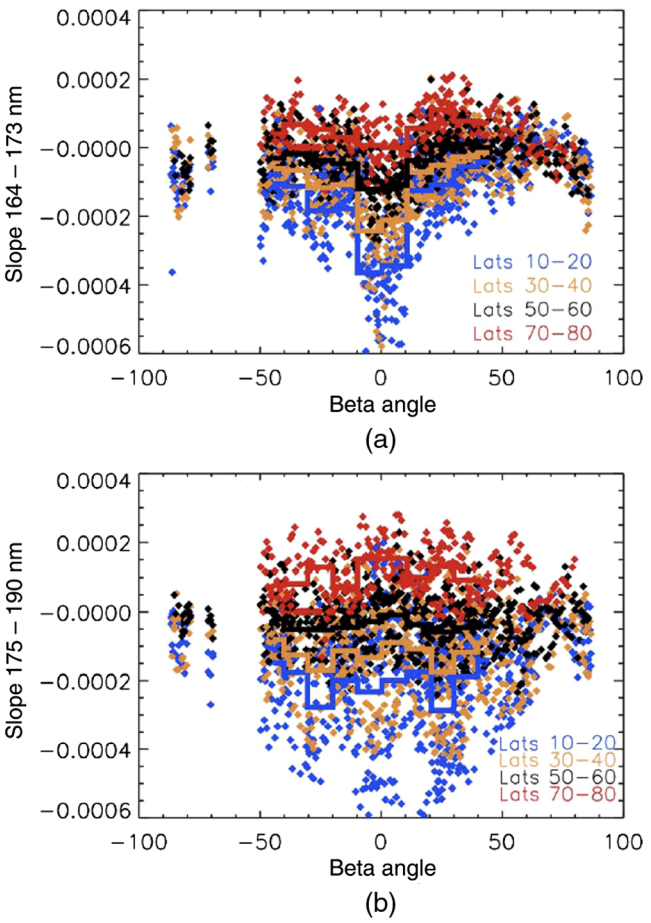

Fig. 3 Measurements of lunar hydration using LAMP.[33] The slope is plotted versus beta angle: (a) 164 to 173 nm and (b) 175 to 190 nm. Negative beta angles correspond to morning, and positive beta angles correspond to afternoon. Average slopes in each 10-deg beta angle range are overplotted as thick lines.

2.3.1 *Clouds of dust in the Moon*

During the Apollo era, astronauts saw horizon glow and streamers in the Moon's outmost atmosphere, or "exosphere." Since then, many scientists have suggested that these phenomena were caused by sunlight scattered by dust grains in the exosphere. Questions about how lunar dust and dusty plasmas are charged, mobilized, and transported remain at the center of dusty plasma studies. EarthASAP is designed to answer these questions by detecting the presence of dust clouds and plumes, as well as their interaction with solar radiation and particles.

3 Mission Concept

The EarthASAP mission covers several science themes devoted to the study of the Earth and the Moon, listed in Table 1. The previous section presented the desired science goals that are achieved by different objectives, which in turn, impose the mission requirements. In Table 1, also the specific results to be obtained are shown.

These scientific requirements can be fulfilled by the EarthASAP proposal, based on 12U cubesat, with 8U dedicated to the scientific payload and 4U to the service module.

3.1 *Scientific Payload*

The optical design of the imager is an evolution of the wide-angle large reflective unobscured system (WALRUS).[36,37] It is a three-element mirror system, with spherical primary and tertiary mirrors and a prolate secondary that results in a system completely free of chromatic aberrations, with a wide field of view (22 deg × 20 deg), focal-ratio of $f/4.5$, and a compact design ($65 \times 115 \times 190$ mm^3) suitable for a cubesat. It also provides an excellent image quality with flat field, covering the spectral range 100 to 300 nm. The optical layout is presented in Fig. 5 and the parameters of the proposed designed are listed in Table 2. Filters will be inserted in a filter wheel before the detector; based on the previous developments,[38–40] a transmittance of 7% with high out-of-band rejection is expected in the narrow band line filters tuned to Lyα, OI, and HeII.

The payload module is assumed to weight 8 kg, consume 4 W, and require a pointing accuracy of 14 arc sec (3σ). Due to the dimensions of the telescope, the payload module requires an 8U system including the detector, an MCP with CMOS read out. The focal length and image size of the telescope are compatible with the use of the multichannel plate PHOTEK image intensifier MCP118,[41] with an input window of MgF_2, a photocathode of CsI and a phosphor anode of P46/P47. The MCP118 image intensifier has a typical effective resolution of 40 to 50 lp/mm, leading to an effective sampling size of around 15 μm and resulting in 2.5 samples inside the optics blur diameter of 0.04 mm. We have checked that it is actually possible to reduce that blur diameter for all points in the field of view to get 500 effective samples across the detector size of 18 mm. The CMOS detector is planned to be an AMS (CMOSIS) 5.5-μm pixel size based on the previous experience.

The encircled energy of the proposed design is included in Fig. 6. As shown, the preliminary optimization performed is enough to bring the optics blur diameter to a value lower than

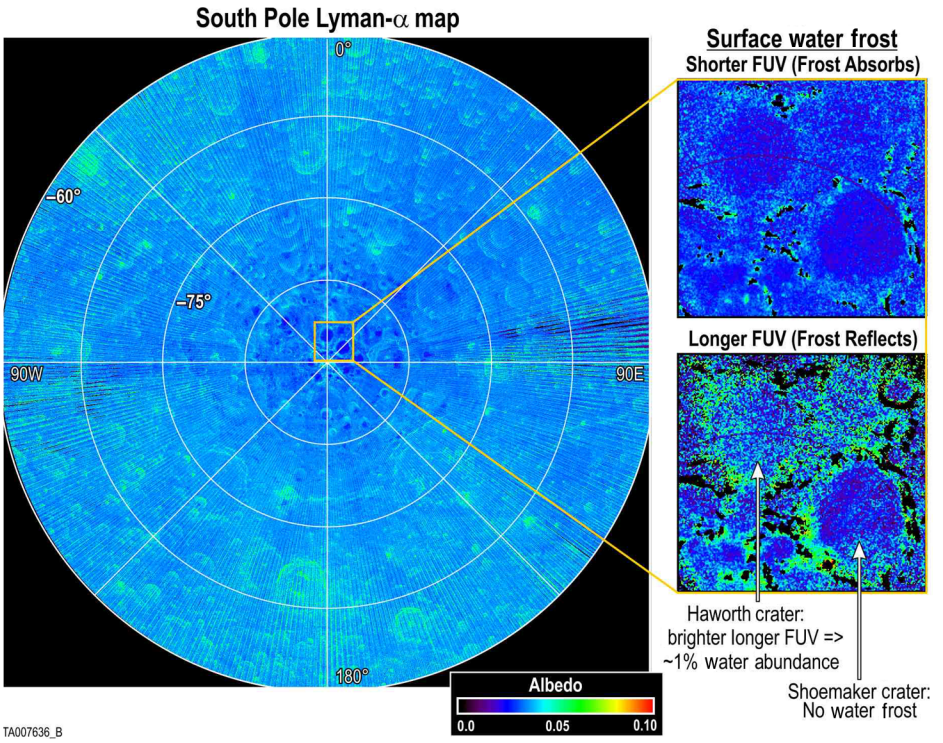

Fig. 4 Measuring the hydration of rocks on the lunar south pole from FUV imaging (courtesy from NASA, LRO/LAMP mission).

0.04 mm, for all points in the field of view. This will result in the optics providing around 500 effective samples across the detector size of 18 mm. The proposed optical design is subjected to a moderate amount of barrel distortion (peak value−4.5%), as can be observed in Fig. 7. This effect will be corrected for as part of the image postprocessing and thus it is not considered relevant in terms of overall optical performance. The simulated effect of both the image quality and optical distortion of the proposed design on the Earth's image is also displayed in this figure.

Sensitivity requirements are met with this design and configuration. The Lyα emission from the Earth's exosphere can be mapped with SNR $>$ 10 up to 15 R_E from the Earth's center. Under the worst conditions (solar zenital angle 90 deg), the exosphere produces a Lyα flux of 0.16 kR at 15 R_E that is observed against a 1.1-kR heliospheric background.[42,43] At the Moon's distance, the count rate from 15 R_E is expected to be 115 counts s^{-1} per angular resolution element (0.05 deg or 335 km^2) at the telescope entry pupil. However, UV optics is not very efficient; the expected transmittance of the optical system at Lyα is about 2% and the detector QE at this wavelength is 30%. As a result, the count rate per angular resolution element on the detector is significantly lower (0.69 counts s^{-1}) and it will be spread in ~6 pixels to sample the PSF by 2.5×2.5 pix^2; SNR = 10 will be reached in <15 min with the optical elements and MCP detectors proposed for EarthASAP. The measurements will be made in TIME-TAG mode with the detector being read every 40 ms; therefore, the total count rate will be 280,000, well within the safety margins of conventional MCP detectors. These calculations are made using state-of-the art technology; the baseline MCP detector is currently under the development for the WSO-UV mission[44] and it is based on the heritage of the ISSIS instrument[45] though its QE has been enhanced to reach the sensitivity of the Hamamatsu detectors used in the LAICA on board the Japanese microspacecraft PROCYON with a rather similar optical configuration.[46] Similar results have also been obtained by SOHO/SWAN.[47]

3.2 *Service Module*

The service module has been sketched selecting some COTS cubesats components listed in Table 3, which will be implemented within four additional units. Therefore, the complete configuration will be a 12U cubesat, $3 \times 2 \times 2$. All these elements, service module, and payload can be integrated in the 12U cubesat as seen in Fig. 8.

4 Observation Strategy and Data Analysis

EarthASAP will map the Earth, its exosphere and magnetosphere, the heliosphere, and the lunar poles with a 20 deg $\times$ 30 deg field imager and an angular resolution of 3 arc min.

The satellite is designed for a low-eccentricity lunar polar orbit, at 500 km of the surface. EarthASAP is designed to communicate with Earth via a lunar orbiter in 800×8000 km polar orbit. Simulating the EarthASAP and the data relay orbiter a daily coverage between 13.5 and 14.5 h is obtained. Figure 9 depicts the EarthASAP data relay lunar orbiter visibility.

The orbital period is 2.64 h. For each orbital period, a basic cycle will be implemented consisting in surveying during 64 min the Earth's exosphere, 12 min the south pole of the Moon, 64 min the heliosphere, and finally 12 min the north lunar pole. This duty cycle is sketched in Fig. 10.

As the orbiter is assumed to provide data relay services, only the fuel to correct the orbit of the cubesat is required. The communications with the lunar orbiter depend on the position in the

Table 1 Scientific goals, requirements, and results traceability matrix.

Theme	Earth interaction with solar wind	
Goal	To observe the Earth's magnetosphere and exosphere in UV	
Specific objectives	Requirements	Results
• Imaging capabilities in FUV range from 115 to 180 nm • To fit the Earth's magnetosphere in one single image • To resolve structures in the Earth's exosphere <0.1 R_E • To observe the spatial distribution of ENAs	• Solar blind detection system in the 115- to 180-nm range • Field of view 22 deg × 20 deg • Angular resolution better than 3 arc min • FUV range, includes Lyα (121.6 nm), OI (130.3 nm), and HeII (164.0 nm) narrow band filtering (FWHM = 5 nm) at these wavelengths is needed	• Production of first 3-D map of Earth's exosphere • Determination of the exospheric emission and transfer function of Lyα photons through the Earth's exosphere
Theme	Diffuse matter within the heliosphere	
Goal	To detect extended features against the heliospheric UV background	
Specific objectives	Requirements	Results
• Detect the 0.16 kR exospheric Lyα emission at 15 R_E over the heliospheric background with SNR = 10 • To resolve structures in the Earth's exosphere <0.1 R_E	• (FoV and angular resolution as above)	• Derivation of the water production rate of a comet as function of time • Produce maps with new extended features such as comet tails, dust clouds, and HI filaments • Planet 9 might be detected if surrounded by a cloud of small bodies and dust from outer Solar System
Theme	Water content on the Moon poles	
Goal	To image lunar hydration, including FUV variability	
Specific objectives	Requirements	Results
• Image the lunar poles • Imaging spots of around 175 km × 260 km • Resolve structures on the lunar surface <0.5 km size • Differential measurements, analysis of FUV slope	• Lunar polar orbit • (FoV and angular resolution as above) • Narrow band filtering at 170, 175, 187, and 190 nm	• Time series of water contents on the Moon's poles
Theme	Space weather on the Moon poles and lunar exosphere	
Goal	To detect the presence of dust clouds and plumes in the lunar exosphere	
Specific objectives	Requirements	Results
• Detect and qualify dust clouds • Detect the 0.16-kR exospheric Lyα emission at 15 R_E over the heliospheric background with SNR = 10	• (FoV and angular resolution as above) • Step filter (f.i,, F_2Ba) to be used together with no-filter to measure extinction • Efficiency of the optical system and aperture	• Confirm if sunlight scattered by dust grains produces the observed features such as horizon glows and streamers

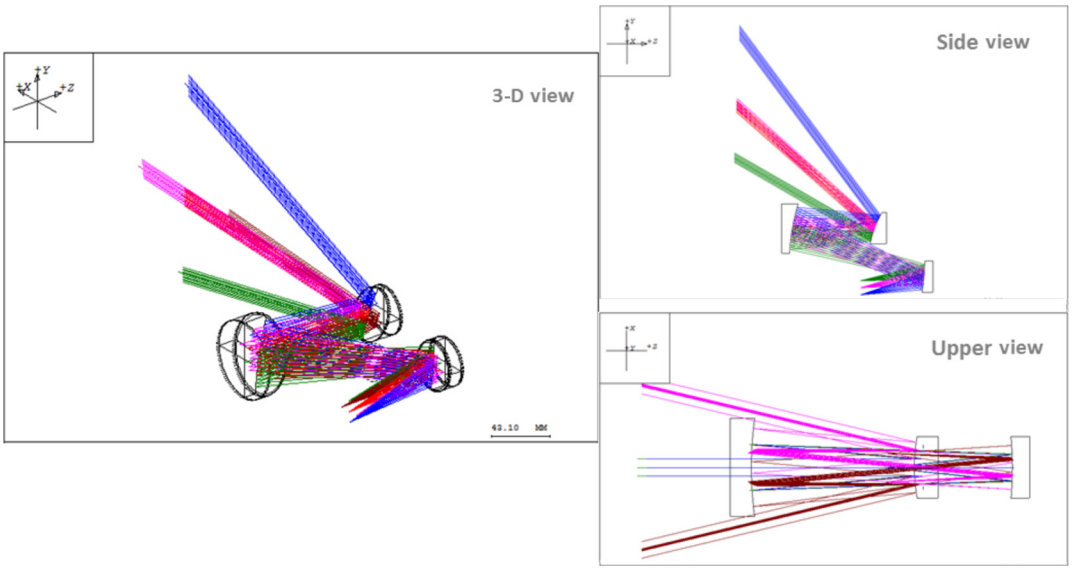

Fig. 5 Optical layout for the WALRUS system implementation.

Table 2 Telescope parameters for the adapted WALRUS system. The stated dimensions correspond only to the presented optical layout, prior to baffling for stray-light control.

Parameter	Value
Type	All-reflective (WALRUS)
Focal length	48 mm
F-number	$f/4.5$
Spectral range	100 to 300 nm
Image size	18 mm
Field of view	(22 deg×20 deg)
Encircled energy diameter	<0.05 deg
Dimensions $(X \times Y \times Z)$	$65 \times 115 \times 190$ mm^3

orbit, but our simulations show that we could obtain a daily coverage between 13.5 and 14.5 h.

The EarthASAP 500-km circular polar orbit will experiment every year two eclipse seasons. Each eclipse season will last about 3.5 months. The maximum eclipse duration will be about 45 min. Statistically, EarthASAP will spend 13.1% of the time in shadow. The mean eclipse duration is 36.6 min with a standard deviation of 9.3 min. In Fig. 11, the EarthASAP yearly eclipse evolution with the daily hours of shadows is depicted.

EarthASAP will produce images at a rate of one frame per minute in different filters. This means around 6048 Mbytes/day. An on-board processing with a compression factor 2 implies total amount of TM of roughly 3629 Mbytes/day. This must be downloaded during the averaged 14 h when the relay spacecraft is visible, following Fig. 9. Presuming a protocol overhead of 20%, the required bandwidth is around 72 kbytes/s. This requirement can be fulfilled using the S-band transmitter listed in Table 3. This proposed S-band transmitter provides 537.5 kbytes/s for downlink, which is enough for our purposes.

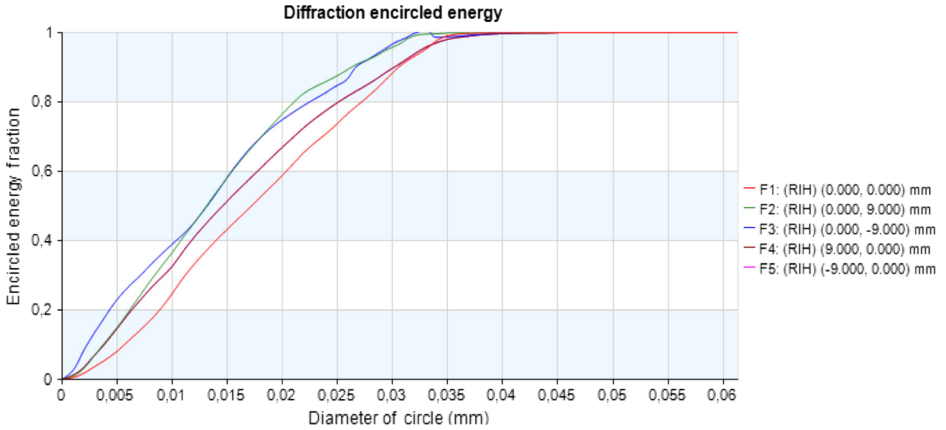

Fig. 6 Encircled energy of the proposed design.

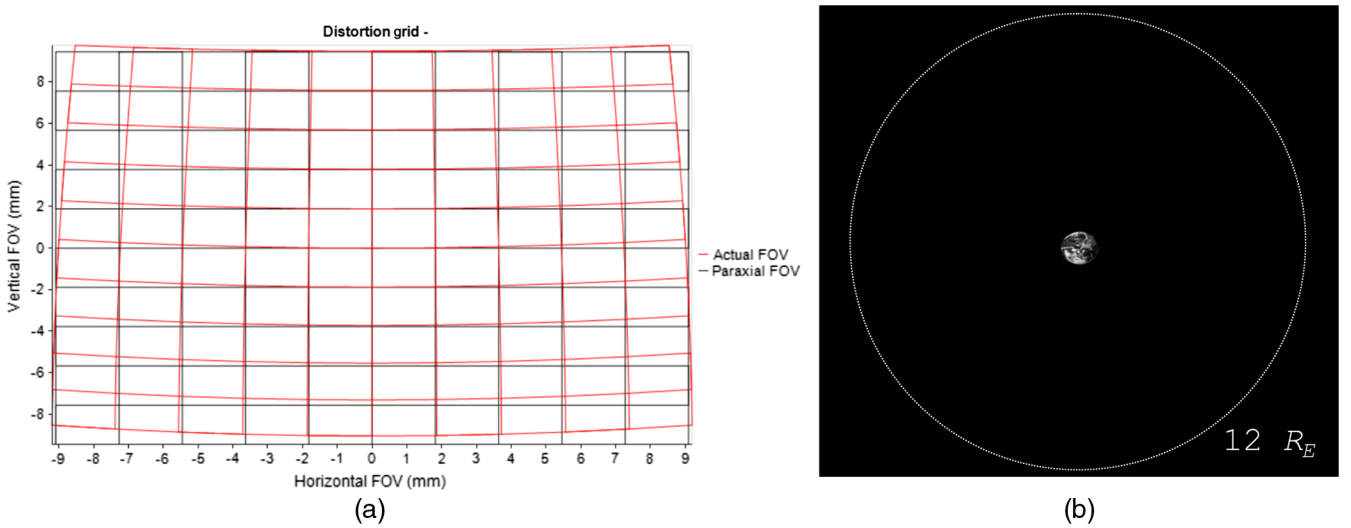

Fig. 7 (a) Optical distortion of the proposed design and (b) simulation of the Earth image as seen with the proposed design.

Table 3 Service module components for EarthASAP.

Unit name	Model and supplier	Mass (g)	Power consumption	Volume (mm^3)
Solar panel	P110A GOMSpace (DK)	29	2300 mW	$98 \times 91.6 \times 5.5$
Star tracker	St-400 hyperion technologies (NL)	280	700 mW steady	$53.8 \times 53.8 \times 90.5$
Reaction wheels	RW400 hyperion technologies (NL)	340	<2500 mW peak	$50 \times 50 \times 27.5$
RCS	GOMSpace (DK)	220	2-W peak, 0.35 W standby	$100 \times 100 \times 30$
On board computer	CP400.85 hyperion technologies (NL)	7	<1000-mW peak	$20 \times 50 \times 10$
Telemetry unit	S-band transmitter ISIS high data rate S-band transmitter (NL)	85	13-W transmitter	$99 \times 93 \times 15$
Battery	NanoPowerBPX GOMSpace (DK)	500		$91.6 \times 85.9 \times 40$

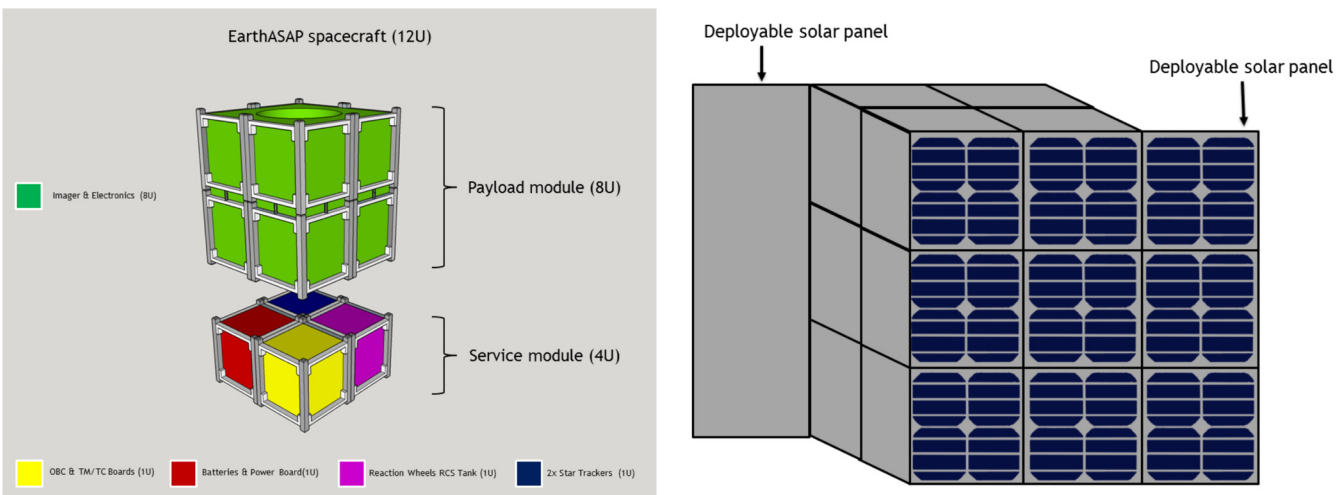

Fig. 8 Integration of the proposed elements of the EarthASAP mission in a 12U cubesat structure.

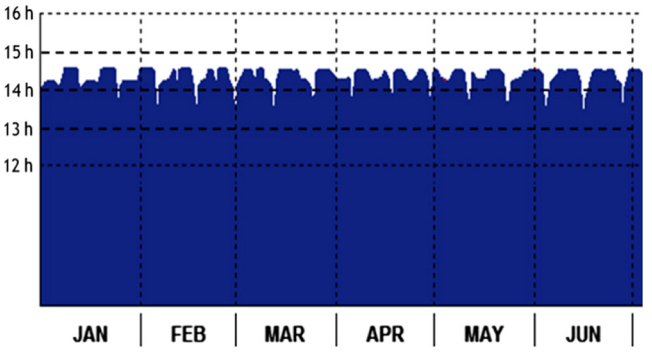

Fig. 9 Estimated EarthASAP data relay Lunar Orbiter Visibility.

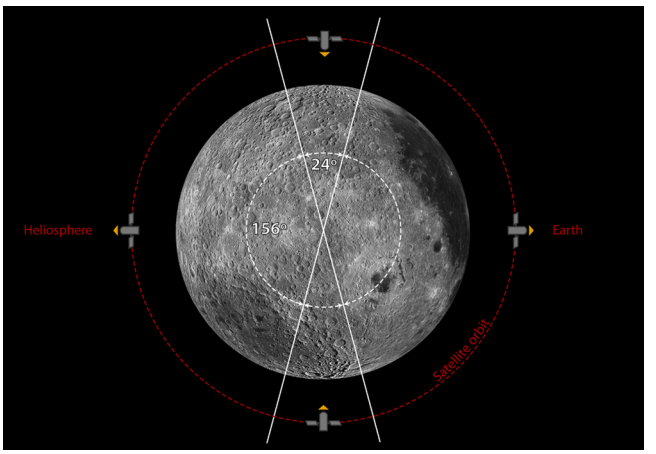

Fig. 10 Mission planning for EarthASAP. Although orbiting the Moon, the satellite will map systematically the Earth's exosphere, the heliosphere, and the lunar poles with an optimized duty cycle.

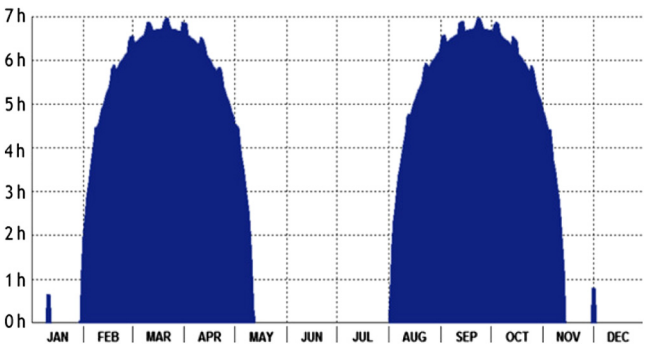

Fig. 11 EarthASAP yearly eclipse evolution.

When defining the duty plan, one must take into account the available power budget, which will determine the activation of the different elements of the spacecraft. For instance, we must consider the power consumption of the selected S-band transmitter or the eclipse seasons. An initial power budget of the service module components and payload is found in Table 4, with a nominal consumption close to 15 W and a peak consumption of 21 W.

The reaction control system (RCS) is needed for unloading the reaction wheels. Periodic maintenance periods will be included in the duty plan to include these activities, when the power consumption may increase. Other periods that can reduce the continuous observations are the eclipses. The batteries can provide just around 5.5 h of full operations. Therefore, during eclipses, if the payload is kept is active, one may decide to interrupt the downlink of data.

Table 4 EarthASAP power budget.

Unit	Peak (W)	Duty cycle (%)	Average (W)
Solar panels (9×)	20.7	70	14.49
Star tracker	−0.7	100	−0.7
Reaction wheels	−2.5	25	−0.6
RCS	−2.0	(When needed)	−0.35
On-board computer	−1.0	100	−1.0
TM/TC unit	−13.0	58	−7.6
Payload	−4.0	100	−4.0

During other periods, no image production will be possible. These periods are, for instance, those when the Sun constraint could be violated because the Sun enters in the FoV of the instrument when observing the Earth. This roughly happen during full moon phases, when no image acquisition is possible. The duty plan can insert maintenance activities here.

4.1 *Data Analysis and Interpretation*

The contamination by cosmic rays will be removed and geometrical distortions will be corrected on board. The optical system is designed to introduce a well-known distortion that will be evaluated on ground tests and reassessed during commissioning. Flat fielding and an additional geometric correction to compensate for the variation of the viewing angle will also be applied on board. Note that the angular velocity of EarthASAP will be $\omega = 2.3$ deg min^{-1}, resulting in a variation of the Earth projected size by a factor cos ωt, which will run faster close to the poles. A final list with event centroids and time will be generated and transferred to Earth for every pointing and filter during a given orbit.

Ground-based processing will include fitting and subtraction of the heliospheric background. Lunar observations and comparison with previous missions (mainly LRO) will be used for flat fielding and calibration. Scattered solar radiation will be the main source for absolute flux calibration.

EarthASAP will take advantage of the wide-field imaging to simultaneously obtain information on solar flux reaching the Earth, the ultraviolet background, and the targets (Earth, Moon, and Solar System) for most objects. Protocols will be implemented to detect and track transient events such as solar flares reaching the Earth, solar storms, and geostorms.

Finally, Lyα maps will be used to map the 3-D structure of the exosphere and determine the transfer of Lyα photons through it. The Lyα source function will be calculated directly from the data and made available to the community for future exo-Earth transit calculations and data interpretation.

5 Summary

This paper summarizes the basic scientific and technological characteristics of a 12U cubesat to be set in lunar orbit. It is shown that the small 8U payload is enough to address important

problems concerning the nature of gas escape from the Earth's atmosphere (and Earth-like planets). The small EarthASAP mission is also well suited to monitor the hydration of the rocks in the lunar poles and the heliosphere. The observatory can be manufactured in few years, at a cost below five million euros.

Up to now, three technical problems have been identified but all can be addressed with the existing technology. First, the proposed optical design is subjected to a moderate amount of barrel distortion. However, this effect can be corrected by the postprocessing of the images. Second, the proposed off-axis telescope requires a lateral input window and a deployable baffle. These two elements might be placed in the side of the payload unit but require designing a structure that allows the window to maintain the structural properties of the system. Also, a baffle or lid would be needed to close the input windows during launch and transit phases. Third, in order to align correctly the off-axis mirror system and maintain it independently of temperature changes, it is fundamental to use materials with small thermal expansion coefficient such as carbon fiber-based composites or inbar.

Most important, to make the Moon accessible to EarthASAP and, in general, to lunar cubesat missions, it is required that a communications relay is set close to the Moon. This is the only means to keep their power needs within the cubesat scale.

Acknowledgments

This paper has been partially funded by the Ministerio de Economia y Competitividad of Spain under Grant No. ESP2015-68908-R.

References

1. http://www.cubesat.org.
2. http://www.exploration.esa.int/moon/59374-overview/.
3. http://www.gsp.esa.int/sysnova.
4. J. Qin and L. Waldrop, "Non-thermal hydrogen atoms in the terrestrial upper thermosphere," *Nat. Commun.* **7**, 13655 (2016).
5. S. A. Fuselier et al., "Overview of the IMAGE science objectives and mission phases," *Space Sci. Rev.* **91**, 51–66 (2000).
6. D. McComas et al., "The two wide-angle imaging neutral-atom spectrometers (TWINS) NASA mission-of-opportunity," *Space Sci. Rev.* **142**, 157–231 (2009).
7. S. Mende et al., "Far ultraviolet imaging from the IMAGE spacecraft. 3. Spectral imaging of Lyman-a and OI 135.6 nm," *Space Sci. Rev.* **91**, 287–318 (2000).
8. J. Chamberlain, "Planetary coronae and atmospheric evaporation," *Planet. Space Sci.* **11**, 901–960 (1963).
9. N. Østgaard et al., "Far ultraviolet imaging from the IMAGE spacecraft. 3. Spectral imaging of Lyman-a and OI 135.6 nm," *J. Geophys. Res. Space Phys.* **108**, 1300 (2003).
10. L. Esposito et al., "The Cassini ultraviolet imaging spectrograph investigation," *Space Sci. Rev.* **115**, 299–361 (2004).
11. S. Werner et al., "UVIS/HDAC Lyman-a observations of the geocorona during Cassinis Earth swing by compared to model predictions," *Adv. Space Res.* **34**, 1647–1649 (2004).
12. J. Zoennchen et al., "The TWINS exospheric neutral H-density distribution under solar minimum conditions," *Ann. Geophys.* **29**, 2211–2217 (2011).
13. A. I. Gomez Castro, L. Beitia-Antero, and S. Ustamujic, "On the feasibility of studying the exospheres of Earth-like exoplanets by Lyman-α monitoring. Detectability constraints for nearby M stars," *Exp. Astron.* **45**, 147–163 (2018).
14. S. Kameda et al., "Ecliptic north-south symmetry of hydrogen geocorona," *Geophys. Res. Lett.* **44**, 11706–11712 (2017).
15. B. D. Shizgal and G. G. Arkos, "Nonthermal escape of the atmospheres of Venus, Earth, and Mars," *Rev. Geophys.* **34**, 483–505 (1996).
16. J. J. Bailey and M. Gruntman, "Investigation of exosphere variations by Lyman-alpha detectors on the TWINS mission," in *AGU Fall Meeting Abstr.*, p. SA51A-2030 (2013).
17. A. Vidal-Madjar et al., "An extended upper atmosphere around the extrasolar planet HD209458b," *Nature* **422**, 143–146 (2003).
18. A. Lecavelier Des Etangs et al., "Evaporation of the planet HD 189733b observed in HI Lyman-α," *Astron. Astrophys.* **514**, A72 (2010).
19. J. R. Kulow et al., "Lyα transit spectroscopy and the neutral hydrogen tail of the hot neptune GJ 436b," *Astrophys. J.* **786**, 132 (2014).
20. D. Ehrenreich et al., "The transmission spectrum of Earth-size transiting planets," *Astron. Astrophys.* **448**, 379–393 (2006).
21. A. I. Gómez de Castro et al., "Protoplanetary disk shadowing by gas infalling onto the young star AK Sco," *Astrophys. J.* **818**, L17 (2016).
22. R. Buick, "The earliest records of life on Earth," in *Planets and Life*, W. T. Sullivan and J. A. Baross, Eds., pp. 237–264, Cambridge University Press, Cambridge (2007).
23. J. Bertaux and J. Blamont, "Evidence for a source of an extraterrestrial hydrogen Lyman-alpha emission," *Astron. Astrophys.* **11**, 200 (1971).
24. G. Thomas and R. Krassa, "OGO 5 measurements of the Lyman alpha sky background," *Astron. Astrophys.* **11**, 218 (1971).
25. E. Stone et al., "Appearance of a third episode of enhanced particle intensities at 94 AU: voyager 1 in the heliosheath," *Int. Cosmic Ray Conf.* **2**, 43 (2005).
26. M. Witte, M. Banaszkiewicz, and H. Rosenbauer, "Recent results on the parameters of the interstellar helium from the ULYSSES/GAS experiment," *Space Sci. Rev.* **78**, 289–296 (1996).
27. R. Rairden, L. Frank, and J. Craven, "Geocoronal imaging with dynamics explorer," *J. Geophys. Res.* **91**, 13613 (1986).
28. J. Bertaux et al., "Lyman-alpha observations of comet Hyakutake with SWAN on SOHO," *Planet. Space Sci.* **46**, 555–568 (1998).
29. J. Mäkinen et al., "Discovery of a comet by its Lyman-a emission," *Nature* **405**, 321–322 (2000).
30. B. Shustov et al., "Comets in UV," *Astrophys. Space Sci.* **363**, 64 (2018).
31. S. A. Stern et al., "Alice: the Rosetta ultraviolet imaging spectrograph," *Space Sci. Rev.* **128**, 507–527 (2007).
32. G. Gladstone et al., "Far-ultraviolet reflectance properties of the moon's permanently shadowed regions," *J. Geophys. Res. Atmos.* **117**, E00H04 (2012).
33. A. R. Hendrix et al., "The lunar far-UV albedo: indicator of hydration and weathering," *J. Geophys. Res. (Planets)* **117**, E12001 (2012).
34. A. R. Hendrix et al., "Lunar swirls: far-UV characteristics," *Icarus* **273**, 68–74 (2016).
35. G. Chin et al., "Lunar reconnaissance orbiter overview: the instrument suite and mission," *Space Sci. Rev.* **129**, 391–419 (2007).
36. K. Hallam, B. Howell, and M. Wilson, "Wide-angle flat field telescope," U.S. Patent No. 4, 598, 981 (1986).
37. K. Hallam, B. Howell, and M. Wilson, "An all-reflective wide-angle flat-field telescope for space," *Proc. SPIE* **445**, 295–301 (1984).
38. L. Rodríguez-de Marcos et al., "Advances in far-ultraviolet reflective and transmissive coatings for space applications," *Proc. SPIE* **9912**, 99122E (2016).
39. A. I. Gómez de Castro et al., "The imaging and slitless spectroscopy instrument for surveys (ISSIS) for the world space observatory-ultraviolet (WSO-UV)," *Astrophys. Space Sci.* **335**, 283–289 (2011).
40. M. Fernández-Perea et al., "Novel narrow filters for imaging in the 50–150 nm VUV range," *Astrophys. Space Sci.* **320**, 243–246 (2009).
41. http://www.photek.com/pdf/datasheets/detectors/DS001_Image_Intensifiers.pdf.
42. W. Pryor et al., "Interplanetary Lyman a observations from Pioneer Venus over a solar cycle from 1978 to 1992," *J. Geophys. Res.* **103**, 26833–26849 (1998).
43. E. Qémerais et al., "Hydrogen atoms in the inner heliosphere: SWAN-SOHO and MASCS-MESSENGER observations," *J. Geophys. Res. Space Phys.* **119**, 8017–8029 (2014).
44. B. Shustov et al., "The world space observatory ultraviolet (WSO-UV), as a bridge to future UV astronomy," *Astrophys. Space Sci.* **363**, 62 (2018).

45. A. I. Gómez de Castro et al., "The imaging and slitless spectroscopy instrument for surveys (ISSIS): expected radiometric performance, operation modes and data handling," *Astrophys. Space Sci.* **354**, 177–185 (2014).
46. S. Kameda, M. Kuwabara, and N. Osada, "Hydrogen Lyman alpha imaging camera onboard PROCYON," in *AGU Fall Meeting Abstr.*, p. P24C-04 (2018).
47. I. I. Baliukin et al., "SWAN/SOHO Lyman-α mapping: the hydrogen geocorona extends well beyond the Moon," *J. Geophys. Res. (Space Phys.)* **124**, 861–885 (2019).

Ana I. Gómez de Castro is a full professor of astronomy and astrophysics in the Universidad Complutense de Madrid (Spain). She leads the Research Group on Space Astronomy and is the principal investigator of the Spanish participation in the Russian-led mission World Space Observatory- UV. She chairs the European Network for Ultraviolet Astronomy and is an elected member of the Steering Committee of Division B (Technology, Facilities and Data Science) in the International Astronomical Union. She has published more than 230 articles on the physics of star formation, interstellar medium, and early stellar evolution.

Leire Beitia-Antero is a PhD student in astrophysics at Complutense University of Madrid (Spain). She studies the propagation of hydromagnetic waves in the envelopes of the molecular clouds, the role of tiny grains in the coupling of the clouds with the galactic magnetic field, and the detectable signature in the ultraviolet range. She is also interested in the interaction between the interstellar medium and the Solar System bodies, mainly the Earth and the Moon.

Carlos E. Miravet-Fuster: Biography is not available.

Lorenzo Tarabini has been system engineer at SENER S.A. since 2008, with experience in complex space systems and, in particular, in satellite design, development, and verification. He worked as system engineer for Proba-3 and SMART-OLEV, a commercial mission to provide in orbit servicing to geostationary telecommunication satellite. Since 2015 he has worked on advanced AOCS missions and technologies (EUCLID, PLATO, SPACE RIDER) and on novel technology research projects (CORA-SAGE, Nano Micro Launch Vehicle Avionics and Electro Dynamic Tether projects).

Albert Tomás joined SENER in 2009, as Space and Astronomy Section head. He has more than 40 years of experience in different engineering disciplines and markets: healthcare, space life science and life support systems, physical science and astronomy. Currently, he is working on system engineering at SENER in optomechanical projects for large ground-based telescopes; he is system engineer in the Weave Translation System and Corrector System projects for the William Herschel telescope, and in the project M2 and M3 Cells for the Extremely Large Telescope.

Juan C. Vallejo is an astrophysicist specialized in data processing and numerical modelling. He worked in the science operations centers of ESA observatories ISO and XMM-Newton. Currently, he is working for the Universidad Complutense de Madrid in the ROSCOSMOS WSOUV/ Spectrum-UV project. His research interests focus on the characterization of the reliability of computer simulations and on the analysis of the role of the viscosity on photoevaporative accretion discs.

Ada Canet is a PhD student in astrophysics at the Complutense University of Madrid (UCM). She is staff member of the UCM AEGORA Research Group on Space Astronomy and collaborates with the activities related to the Spanish participation in the World Space Observatory-UV project. Her PhD project focuses on the study of the interaction between stellar winds and Earth-like exospheres, and the characterization of exoplanetary environment.

Mikhail Sachkov professor of the Russian Academy of Sciences, deputy-director of the Institute of Astronomy RAS, co-PI of the World Space Observatory-Ultraviolet mission (1.7 m main telescope aperture for operation in UV spectral range in the period 2025-2035). He has published more than 150 articles. He was an editor of a special issue on UV astronomy of the journal *Astrophysics and Space Science*. His main research interests are the spectroscopy of pulsating stars, spectroscopic instrumentation and space sciences.

Shingo Kameda is full professor in the Department of Physics of Rikkyo University (Japan) and leads the UV Spectroscopy for Exoplanets Working Group in JAXA. He is PI of telescopic camera (TENGOO) and the wide-angle multi-band camera (OROCHI) onboard Martian Moons eXoplaration (MMX) JAXA mission, sub-PI of Hayabusa2's Optical Navigation Camera and lead Co-I of the Mercury Sodium Atmosphere Spectral Imager (MSASI) onboard BepiColombo MIO space- craft. He was PI of Lyman Alpha Imaging Camera (LAICA) onboard PROCYON spacecraft. He has published more than 100 articles. His principal research interests are the origin of planets and planetary system (including exoplanetary science).